Figures and Tables Guidelines

M. Staszewski*, K. Dug and J. Pietraszewicz

Institute of Physics, Polish Academy of Sciences, al. Lotników 32/46, PL-02668 Warsaw Poland

*e-mail: masta@ifpan.edu.pl

1. Figures

For the sake of aesthetics, clarity and readability please follow the guidelines below:

- The preferred file format depends on its type:
  - For vector drawings (images created from geometric shapes such as points, lines, curves, polygons), preferred formats are vector graphics formats (e.g., .eps, .pdf, .svg). This includes such elements as line graphs, charts, plots. Raster graphics should be avoided in this case. If this is not possible, the minimum width of the image should be 8 cm at a resolution of 1000 dpi, i.e., the minimum width should be about 3200 px.
  - For bitmap images, e.g., photographs, SEM images, preferred formats are raster graphics formats (e.g., .png, .tiff, .jpeg, .bmp). The minimal width of the image should be 8 cm with a resolution of 600 dpi, i.e., the minimal width should be approximately 1900 px.
- In the case of figures containing important small details, they could be placed in two columns with the maximal width of 16 cm.
- Each figure should be numbered with Arabic numbers, i.e., 1, 2, 3, etc. When there are several smaller panels within one figure, each of them should be labelled with small letters of the alphabet, i.e., (a), (b), etc.
- The proportions of the figures should be preserved (do not stretch or narrow the height in relation to the width and vice versa)
- High contrast of the image ensures good readability. Try to use the most contrasting colours (e.g., black and white) and use shapes to show different flows.
- Font size and line thickness should be selected in such a way that they do not reduce the legibility of the figure and its aesthetics. After scaling the drawing to one or two columns, fonts should correspond approximately to the size of the fonts in the main text, and not be larger than that.
- Figure labelling must be consistent with the rest of the paper. Use the same abbreviations and symbols. Please use abbreviations rather than whole words.
- Placing any tables in the figure area is forbidden.
- Use $\times$ as a symbol of multiplication, if such is necessary.
- The decimal point should be used rather than a decimal comma, i.e., 0.2 not 0,2.
- Numbers in labels should use the explicit exponential form: 10^4, not E-4.
- Units should be given in square brackets.
- If possible, the legend should be placed within the graph. The description of the panels should be in the caption, not in the figures.

2. Tables

The guidelines for formatting the tables are as follows:

- Tables should be numbered with uppercase Roman numbers in order they appear in the main text.
- The table can fit in one or two columns of the text. Extra wide tables can be rotated 90 degrees and take the whole page. If the table is too large to fit in one page, it can be continued in the next one. If the table is extensive and take up more pages please consider including it in the supplement rather than in the main text.
- Symbols not defined in the main text should be explained in the caption.
- Column headings should be simple and concise, and they should contain units.
- Use a single horizontal rule to separate the column headings from the entries in the table. It can be also used to separate the group of entries.
- Use lowercase Roman letters in superscript for footnotes placed at the bottom of the table and separated by a horizontal rule.

3. Examples

Here are the examples of properly formatted figures and tables. Figures 1-11 were originally published in [1–7, 10, 14, 16] and Tables I–VII in [8, 9, 11–13, 15].

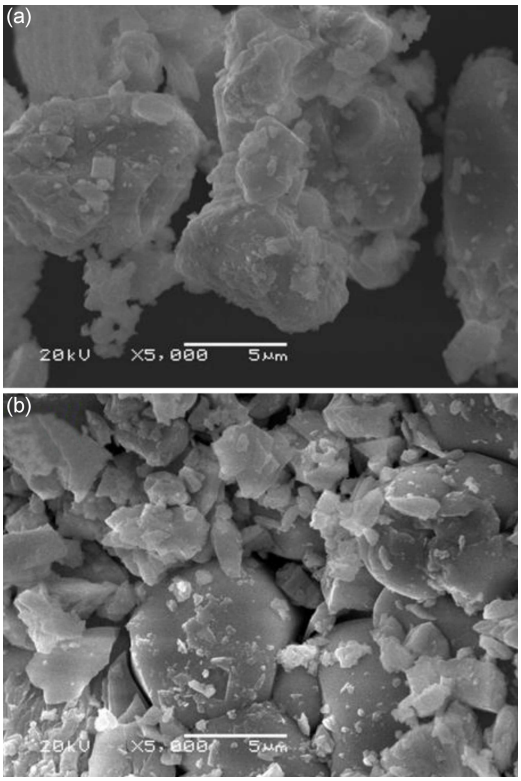

Fig. 1. SEM images of $K_{0.45}Bi_{0.55}Mo_{0.9}V_{0.1}O_4$ and $K_{0.45}Bi_{0.40}Eu_{0.15}Mo_{0.9}V_{0.1}O_4$ samples. (Fig. 2 from [1]).

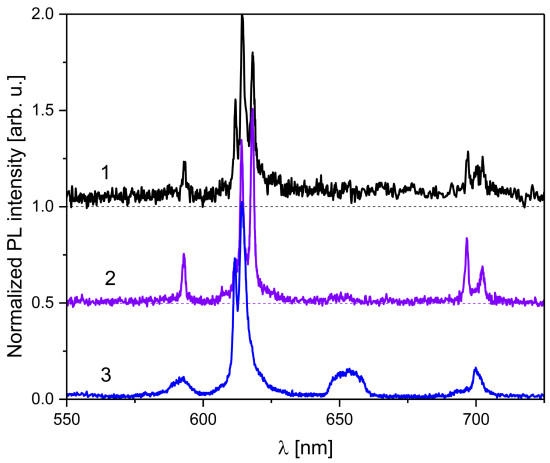

Fig. 2. Photoluminescence spectra of $K_{0.45}Bi_{0.40}Eu_{0.15}Mo_{0.9}V_{0.1}O_4$ solid solution obtained for excitation at λ_{ex} = 320 nm (1), 396 nm (2) and 473 nm (3) at room temperature. Zero intensity levels for spectra 1 and 2 are shown by dashed lines. (Fig. 3 from [1]).

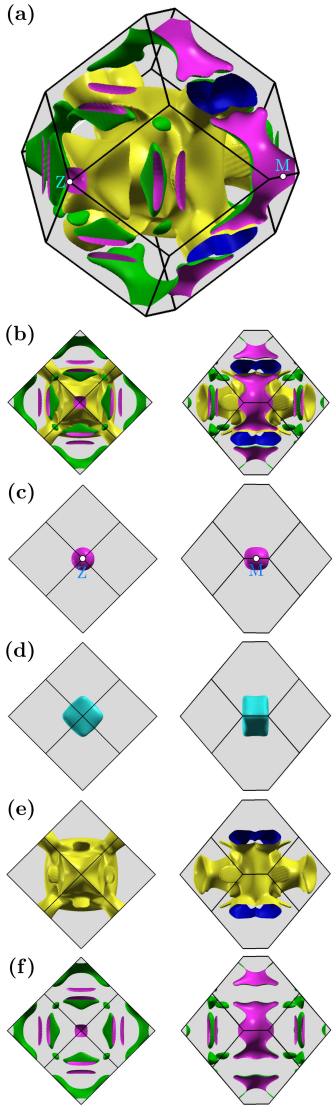

Fig. 3. The Fermi surface of Pb_2Pd with $I4/mcm$ symmetry in the presence of spin–orbit coupling. Panels (a) and (b) present the full Fermi surface, while panels (c)–(f) present separate pockets. (Fig. 3 from [2]).

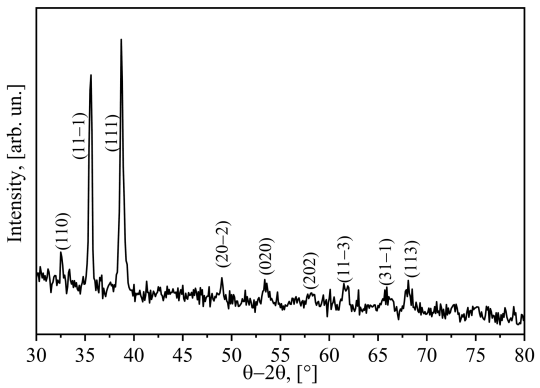

Fig. 4. XRD patterns of CuO film deposited on glass substrate. (Fig. 1 from [3]).

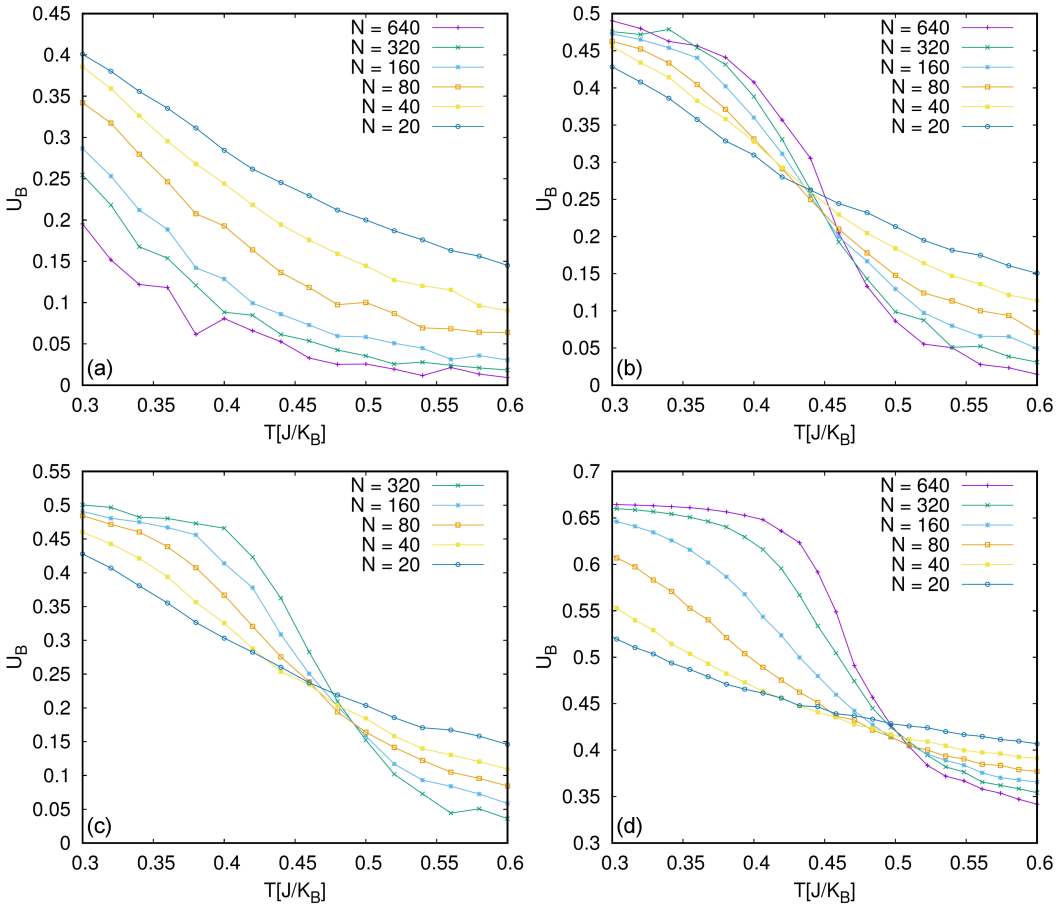

Fig. 5. Binder cumulant for variable-range ξ values, i.e., (a) $\xi = 1.3$, (b) $\xi = 1.4$, (c) $\xi = 1.6$, (d) (d) $\xi = 2$ full coupling (HMF model). (Fig. 3 from [4]).

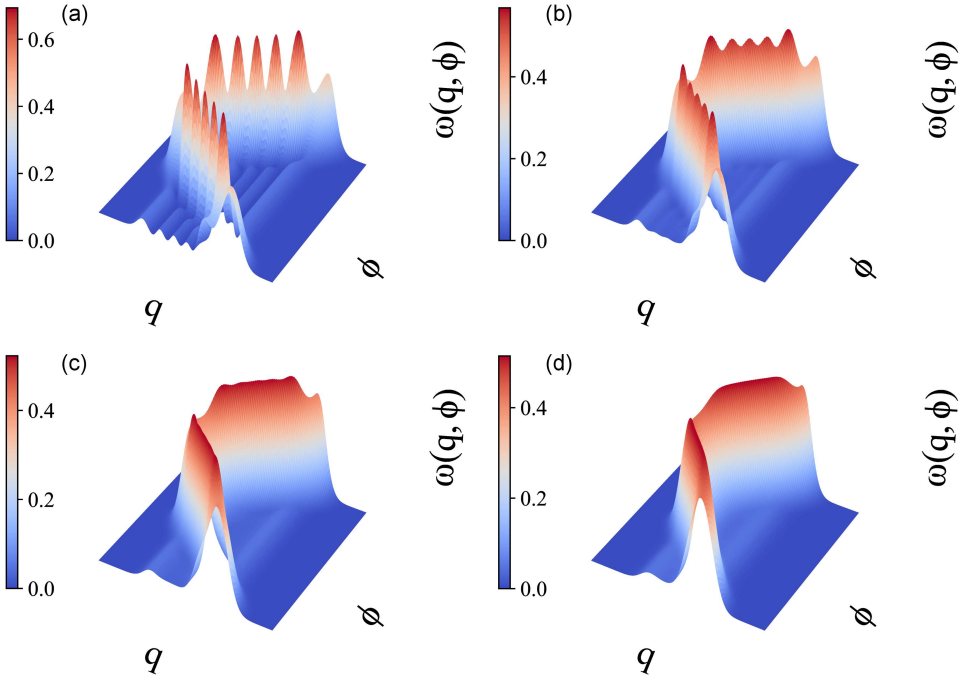

Fig. 6. Degradation of optical tomogram pattern from unit quantum efficiency ($\eta = 1$ (a)) to non-unit quantum efficiency ($\eta = 0.8$ (b), $\eta = 0.6$ (c), $\eta = 0.4$ (d)) for $|\alpha|^2 = n = 5$. (Fig. 3 from [5]).

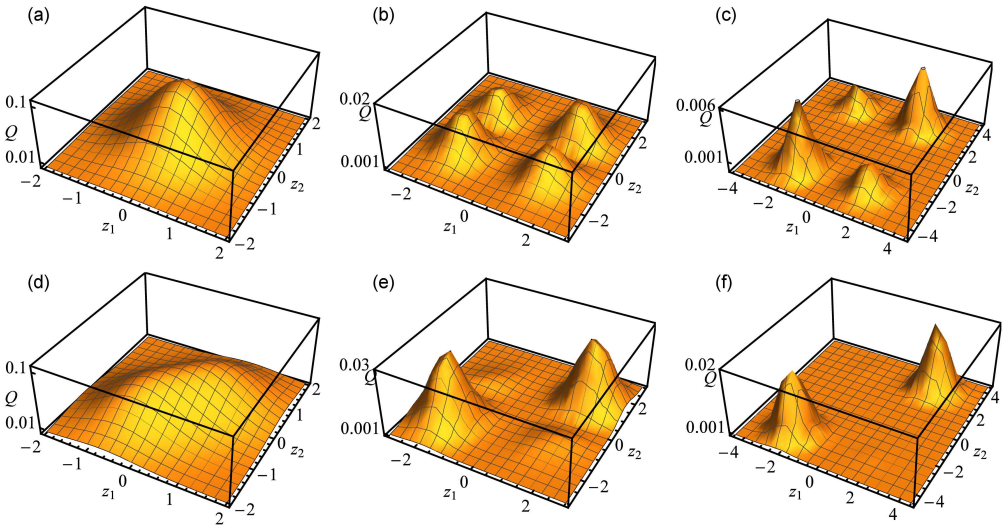

Fig. 7. Q-function of $|\psi_1^+(\alpha, m, n)\rangle$ for different values of photon-excitations $m = n = 0$ in (a) and (d), $m = 2$, $n = 1$ in (b) and (e), $m = 3$, $n = 7$ in (c) and (f) respectively, and for fixed values of $|\alpha|^2$ ($|\alpha|^2 = 0.05$ in upper row and $|\alpha|^2 = 0.5$ in lower row) (Fig. 3 from [6]).

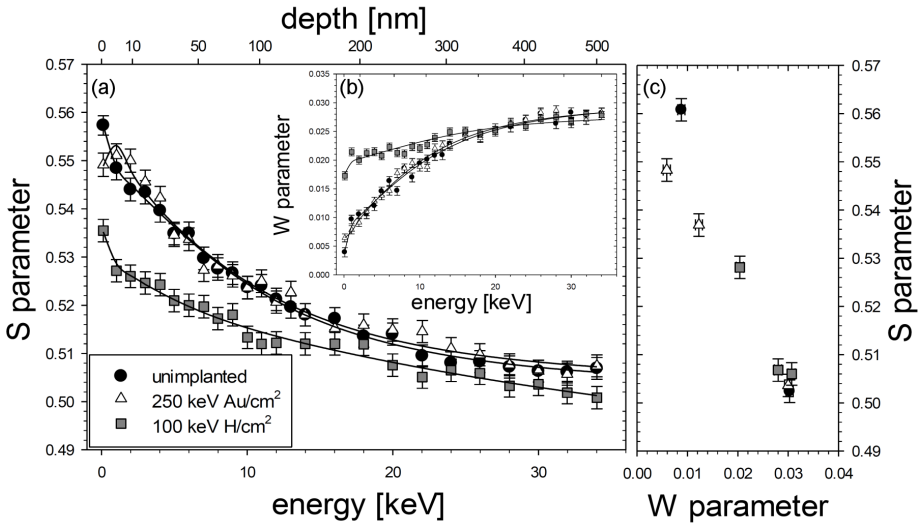

Fig. 8. The measured parameter S (a) and parameter W (b) as a function of the positron incident energy for the studied samples. The top axis in (a) represents the mean positron implantation depth. The solid lines represent the best fit of the experimental points using the VEPFIT code. The W parameter versus the S parameter is obtained from VEPFIT fitting in (c). (Fig. 2 from [7]).

TABLE I

Average oxide thickness in mm of specimen after 25 h furnace atmosphere–air (765°C) exposures. (Table IV from [8])

Specimen (Mn [wt%])	Specimen thickness [mm]	Oxide depth [mm]			Total depth of attack [mm]	Percentage depth of attack [%]
		1st layer — outer	2nd layer —inner	3rd layer —inner		
12	15	0.1570	0.0991	0.0493	0.3054	2.04
11	15	0.1630	0.1250	0.0554	0.3434	2.29
10	15	0.1700	0.1170	0.0696	0.3566	2.38
9	15	0.1720	0.1350	0.0920	0.3990	2.66

TABLE II

New leave one out DFA compared with the traditional DFA, fractional Gaussian noise with length $n = 10000$. (Table III from [9])

Largest window $g(n)$	Hurst exponent	Leave one out DFA				Traditional DFA			
		Mean	Bias	MSE	Var	Mean	Bias	MSE	Var
$\ln(n)^2$	0.10	0.14847571	0.04847571	0.002366881	0.000017158	0.148754658	0.048754658	0.002394289	0.0000174471
	0.15	0.191958353	0.041958353	0.001789245	0.000029032	0.19247952	0.04247952	0.001833765	0.0000295508
	0.20	0.236371835	0.036371835	0.001365115	0.000042631	0.237164892	0.037164892	0.001424273	0.0000434782
	0.25	0.281618247	0.031618247	0.001056593	0.000057454	0.282687201	0.032687201	0.001126496	0.000058630
	0.30	0.327591805	0.027591805	0.000833591	0.000073013	0.328934400	0.028934400	0.000910999	0.000074545
	0.35	0.374191569	0.024214199	0.000673336	0.000088994	0.375806297	0.025806297	0.000755923	0.000090867
	0.40	0.421329026	0.021588285	0.000559018	0.000105143	0.423214337	0.023412759	0.000645148	0.000107316
	0.45	0.468927727	0.019474147	0.000478240	0.000121193	0.471080994	0.021532355	0.000566844	0.000123672
	0.50	0.516919489	0.017786878	0.000421916	0.000137017	0.519338920	0.020052287	0.000512361	0.000139764
	0.55	0.565245525	0.016486940	0.000383378	0.000152477	0.567929941	0.018905322	0.000475388	0.000155460
	0.60	0.613855530	0.015677813	0.000357762	0.000167461	0.616803899	0.018052666	0.000451323	0.000170659
	0.65	0.662706797	0.015230659	0.000341516	0.000181872	0.665917243	0.017547238	0.000436788	0.000185283
	0.70	0.711759932	0.014981687	0.000331962	0.000195623	0.715230870	0.017273016	0.000429238	0.000199251
	0.75	0.760975126	0.014852554	0.000326944	0.000208577	0.764705720	0.017174421	0.000426559	0.000212425
	0.80	0.810301426	0.014761404	0.000324294	0.000220378	0.814291072	0.017141093	0.000426434	0.000224443
	0.85	0.858209069	0.012727241	0.000270590	0.000205254	0.862441356	0.014866938	0.000361170	0.000208467
	0.90	0.907835716	0.012782651	0.000276950	0.000217728	0.912319327	0.015000363	0.000370455	0.000220898
	0.95	0.957574223	0.012987327	0.000285562	0.000230498	0.962307902	0.015179477	0.000382819	0.000233671

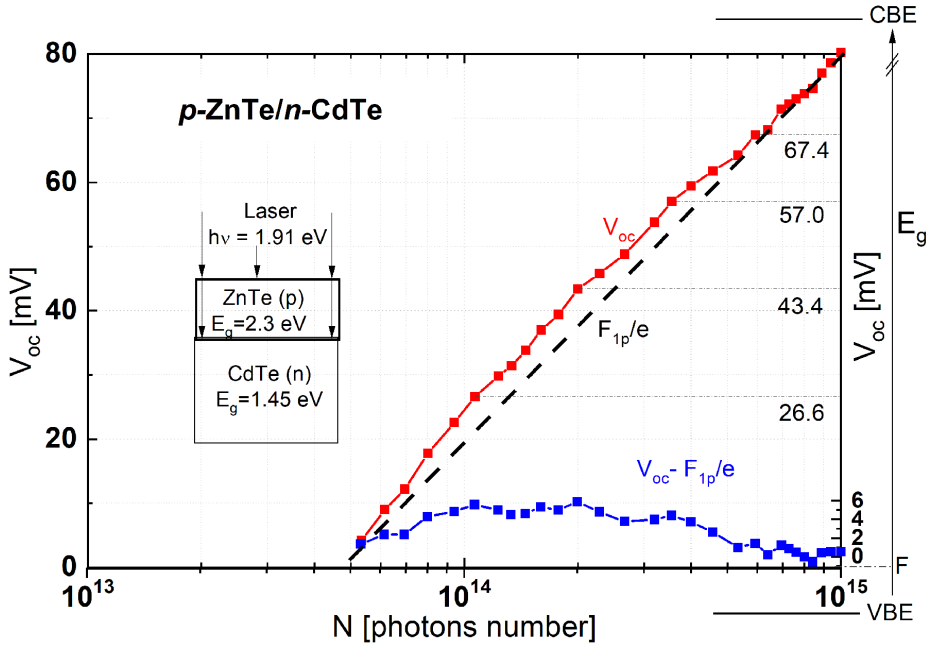

Fig. 9. The comparison of the experimental and theoretical V_{oc} versus illumination intensity curve for the p-ZnTe/n-CdTe of photocell. The heterojunction is illuminated from the ZnTe side with photon bunches of energy $h\nu = 1.91$ eV coming from the laser. The ZnTe layer ($E_g = 2.3$ eV) is transparent to the light and absorbed by the CdTe ($E_g = 1.45$ eV) layer. The red curve presents measured experimental V_{oc} values for different illumination intensity. The black dashed line presents the V_{oc} values predicted by the model for different illumination intensity, while the blue curve presents the difference between the experimental and the model curves. The peaks visible in the lowest curve, as well as the steps on the experimental curve illustrate the effect of extending defects states influencing the V_{oc} value. The right hand side energy scale indicates the steps of the quasi Fermi level energy position corresponding to the measured V_{oc} values of 26.6, 43.4, 57.0, and 67.4 meV located below the thermal equilibrium Fermi level $F = 0$. (Fig. 3 from [10]).

TABLE III

Transition probabilities (A_{ji}), weighted oscillator strengths (gf), and wavelengths (λ) for electric dipole (E1) transitions between the levels of $3l$ (l = 0, 1, 2) and $4l$ (l = 0, 1, 2, 3) in Pb^{+71}. Numbers in brackets represent powers of 10. (Table III from [11])

Transitions				Method	A_{ji} [s^{-1}]		gf		λ [Å]		S [a. u.]
Upper level		Lower level			This work	Other works	This work	Other works	This work	Other works	This work
$3p$	$^2P^o_{1/2}$	$3s$	$^2S_{1/2}$	AUTOS.	5.75(10)	3.515(10)[a]	7.35(−2)	7.02(−2)[b]	65.29	65.854[d]	1.58(−2)
				HFR	5.98(10)	5.375(10)[b]	7.77(−2)	7.1142(−2)[c]	65.85	65.846[e]	1.69(−2)
$3p$	$^2P^o_{3/2}$	$3s$	$^2S_{1/2}$	AUTOS.	4.56(12)	4.569(12)[a]	6.57(−1)	6.628(−1)[a]	15.51	15.5218[d]	1.68(−2)
				HFR	4.56(12)	4.545(12)[b]	6.59(−1)	6.6484(−1)[c]	15.52	15.515[e]	1.68(−2)
$3d$	$^2D_{3/2}$	$3p$	$^2P^o_{1/2}$	AUTOS.	3.55(12)	3.542(12)[a]	4.87(−1)	4.822(−1)[a]	15.12	–	1.21(−2)
				HFR	3.95(12)		4.99(−1)	4.8272(−1)[c]	15.22		1.37(−2)
$3d$	$^2D_{3/2}$	$3p$	$^2P^o_{3/2}$	AUTOS.	1.17(10)	1.204(10)[a]	2.43(−2)	2.458(−2)[a]	58.94	–	4.73(−3)
				HFR	1.13(10)		2.50(−2)	2.4672(−2)[c]	60.76		5.00(−3)
$3d$	$^2D_{5/2}$	$3p$	$^2P^o_{3/2}$	AUTOS.	3.43(11)	3.355(11)[a]	3.82(−1)	3.814(−1)[a]	35.17	–	2.95(−2)
				HFR	3.38(11)		3.84(−1)	3.8162(−1)[c]	35.57		3.00(−2)
$4s$	$^2S_{1/2}$	$3p$	$^2P^o_{1/2}$	AUTOS.	2.71(13)	2.663(13)[a]	7.55(−2)	1.968(−1)[a]	3.05	–	0.76(−3)
				HFR	5.48(13)	2.767(13)[b]	1.58(−1)		3.10		1.61(−3)
$4s$	$^2S_{1/2}$	$3p$	$^2P^o_{3/2}$	AUTOS.	9.95(13)	8.486(13)[a]	3.85(−1)	3.410(−1)[a]	3.59	–	9.09(−3)
				HFR	6.66(13)	8.594(13)[b]	2.68(−1)		3.66		6.45(−3)
$4p$	$^2P^o_{1/2}$	$3s$	$^2S_{1/2}$	AUTOS.	9.42(13)	1.034(14)[a]	2.32(−1)	2.626(−1)[a]	2.87	–	2.20(−3)
				HFR	7.80(13)		3.51(−1)		2.74		1.58(−3)
$4p$	$^2P^o_{1/2}$	$3d$	$^2D_{3/2}$	AUTOS.	2.65(13)	2.922(13)[a]	1.11(−1)	1.274(−1)[a]	3.74	–	2.74(−3)
				HFR	2.00(13)		8.73(−2)		3.81		2.18(−3)
$4p$	$^2P^o_{1/2}$	$4s$	$^2S_{1/2}$	AUTOS.	1.05(10)	1.325(12)[a]	9.76(−2)	1.038(−1)[a]	175.94	–	5.64(−2)
				HFR	1.00(10)		9.83(−2)		181.07		5.86(−2)
$4p$	$^2P^o_{3/2}$	$3s$	$^2S_{1/2}$	AUTOS.	5.43(13)	5.388(13)[a]	2.39(−1)	2.258(−1)[a]	2.71	–	1.07(−3)
				HFR	7.80(13)		3.51(−1)		2.74		1.58(−3)
$4p$	$^2P^o_{3/2}$	$3d$	$^2D_{3/2}$	AUTOS.	1.33(12)	1.428(12)[a]	9.63(−3)	1.074(−2)[a]	3.47	–	1.10(–4)
				HFR	2.54(12)		1.89(−2)		3.52		2.19(−4)
$4p$	$^2P^o_{3/2}$	$3d$	$^2D_{5/2}$	AUTOS.	1.59(13)	1.551(13)[a]	1.24(−1)	1.052(−1)[a]	3.62	–	2.23(−3)
				HFR	2.02(13)		1.63(−1)		3.67		2.96(−3)
$4p$	$^2P^o_{3/2}$	$4s$	$^2S_{1/2}$	AUTOS.	1.09(12)	1.090(12)[a]	9.37(−1)	9.416(−1)[a]	37.87	–	5.84(−2)
				HFR	1.20(12)		9.69(−1)		36.76		5.88(−2)
$4d$	$^2D_{3/2}$	$3p$	$^2P^o_{1/2}$	AUTOS.	1.50(14)	1.400(14)[a]	6.90(−1)	6.656(−1)[a]	2.77	–	3.15(−3)
				HFR	2.09(14)		9.96(−1)		2.82		4.63(−3)
$4d$	$^2D_{3/2}$	$3p$	$^2P^o_{3/2}$	AUTOS.	3.65(13)	3,320(13)[a]	2.26(−1)	2.126(−1)[a]	3.21	–	2.38(−3)
				HFR	2.68(13)		1.72(−1)		3.27		1.85(−3)
$4d$	$^2D_{3/2}$	$4p$	$^2P^o_{1/2}$	AUTOS.	1.06(12)	9.878(11)[a]	8.59(−1)	8.332(−1)[a]	36.76	–	5.20(−2)
				HFR	1.08(12)		8.78(−1)		36.87		5.34(−2)
$4d$	$^2D_{3/2}$	$4p$	$^2P^o_{3/2}$	AUTOS.	2.85(9)	2.863(9)[a]	4.07(−2)	4.064(−2)[a]	154.29	–	2.07(−2)
				HFR	1.74(9)		3.53(−2)		183.77		2.13(−2)
$4d$	$^2D_{5/2}$	$3p$	$^2P^o_{3/2}$	AUTOS.	2.09(14)	1.862(14)[a]	1.87(0)	1.734(0)[a]	3.16	–	1.30(−2)
				HFR	1.69(14)		1.57(0)		3.22		1.11(−2)
$4d$	$^2D_{5/2}$	$4p$	$^2P^o_{3/2}$	AUTOS.	9.76(10)	9.208(10)[a]	6.66(−1)	6.550(−1)[a]	87.09	–	1.27(−1)
				HFR	7.32(10)		6.07(−1)		96.02		1.28(−1)
$4f$	$^2F^o_{5/2}$	$3d$	$^2D_{3/2}$	AUTOS.	3.85(14)	3.682(14)[a]	3.78(0)	3.756(0)[a]	3.30	–	2.73(−2)
				HFR	3.90(14)		3.96(0)		3.36		2.92(−2)
$4f$	$^2F^o_{5/2}$	$3d$	$^2D_{5/2}$	AUTOS.	2.63(13)	2.511(13)[a]	2.79(−1)	2.762(−1)[a]	3.43	–	3.14(−3)
				HFR	2.47(13)		2.72(−1)		3.50		3.14(−3)
$4f$	$^2F^o_{5/2}$	$4d$	$^2D_{3/2}$	AUTOS.	2.30(10)	2.066(10)[a]	2.96(−1)	2.848(−1)[a]	119.76	–	7.80(−2)
				HFR	2.25(10)		2.96(−1)		120.92		7.85(−2)

TABLE III cont.

Transitions				Method	A_{ji} [s^{-1}]		gf		λ [Å]		S [a. u.]
Upper level		Lower level			This work	Other works	This work	Other works	This work	Other works	This work
$4f$	$^2F^o_{5/2}$	$4d$	$^2D_{5/2}$	AUTOS.	1.04(8)	1.015(8)^a	8.32(−3)	8.232(−3)^a	298.59	–	8.20(−3)
				HFR	1.02(8)		8.42(−3)		303.32		8.43(−3)
$4f$	$^2F^o_{7/2}$	$3d$	$^2D_{5/2}$	AUTOS.	4.00(14)	3.807(14)^a	5.58(0)	5.503(0)^a	3.41	–	4.70(−2)
				HFR	3.79(14)		5.48(0)		3.47		4.69(−2)
$4f$	$^2F^o_{7/2}$	$4d$	$^2D_{5/2}$	AUTOS.	6.95(9)	6.740(9)^a	2.78(−1)	2.744(−1)^a	182.44	–	1.25(−1)
				HFR	6.84(9)		2.78(−1)		183.93		1.26(−1)

^{a}Ref. [10], ^{b}Ref. [14], ^{c}Ref. [18], ^{d}Ref. [17], ^{e}Ref. [9]

TABLE IV

The final experimental trial of optimization processing of LTAPJ.(Table I from [12])

Deadband range [μs]	Current [A]	Voltage [V]	Stability	Plasma dose [J]
0.72	5.00	13.0	✓	26.0
2.66	2.40	13.0	✓	9.1
1.53	5.00	11.5	✓	23.0
0.90	5.00	13.7	✓	27.4
1.22	2.30	12.8	✓	8.3
1.40			×	
1.58	4.00	13.4	✓	20.1
1.71	3.00	13.0	✓	13.0
2.17	2.60	12.8	✓	10.2
2.75	2.34	12.8	✓	8.6
3.00	2.17	12.8	✓	7.5
3.11			×	
3.25	2.15	12.8	✓	7.4
8.80	2.08	12.8	✓	6.9
6.90			×	
2.44	2.60	12.8	✓	10.2

TABLE V

Transverse vibration frequencies of the discrete-continuous model of the exoskeleton's lower limb in the xw plane (structure made of 1060 Alloy). (Table III from [13])

	$\alpha = 90°$, $\beta = 180°$			$\alpha = 45°$, $\beta = 90°$		
m [kg]	50	60	70	50	60	70
$K_w = K_y = C_{wy} = 1 \times 10^8$ N/m						
ω_1 [Hz]	0.88	0.78	0.70	1.48	1.33	1.21
ω_2 [Hz]	50.75	50.52	50.29	26.39	26.18	25.97
ω_3 [Hz]	180.2	178.7	177.2	209.2	206.4	203.6
$K_w = K_y = C_{wy} = 1 \times 10^{15}$ N/m						
ω_1 [Hz]	1.41	1.27	1.16	1.98	1.79	1.64
ω_2 [Hz]	61.58	61.31	61.05	38.69	38.22	37.75
ω_3 [Hz]	194.4	192.7	191.0	221.6	218.3	215.2

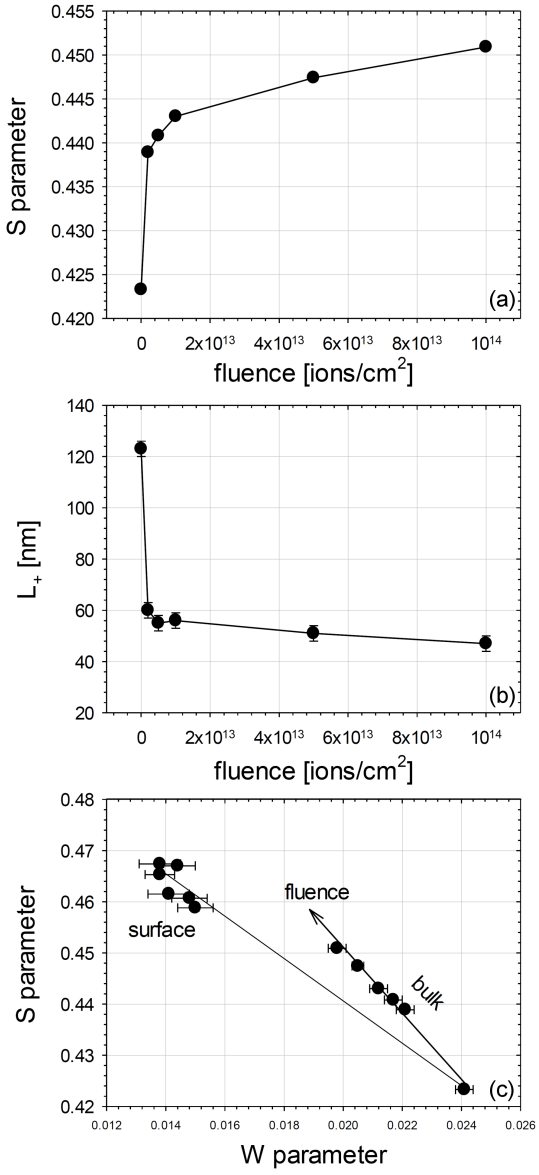

Fig. 10. Values obtained from fitting profiles shown in Fig. 2 using the VEPFIT code, plotted as: S parameter for saturation of $S(E)$ distributions versus dose (a), positron diffusion length depending on the dose (b) and $W(S)$ (c). (Fig. 3 from [14]).

TABLE VI

The main optical transitions and imaginary part peaks of Cs_2SnBr_6 and Rb_2SnBr_6. (Table VI from [15])

Peaks	$W \to L$	$L \to \Gamma$	$\Gamma \to X$	$X \to W$	$W \to K$
			Cs_2SnBr_6		
$E = 2.64$ eV	$V_1 \to C_1$, $V_2 \to C_1$, $V_3 \to C_1$	$V_5 \to C_1$, $V_6 \to C_1$	$V_6 \to C_1$, $V_5 \to C_1$, $V_3 \to C_1$		
$E = 5.34$ eV	$V_1 \to C_3$, $V_2 \to C_3$, $V_3 \to C_3$, $V_4 \to C_3$, $V_6 \to C_3$	$V_5 \to C_3$, $V_6 \to C_3$, $V_1 \to C_4$, $V_3 \to C_4$, $V_1 \to C_6$	$V_1 \to C_4$, $V_1 \to C_6$, $V_3 \to C_6$		
$E = 6.74$ eV	$V_3 \to C_4$, $V_4 \to C_4$, $V_5 \to C_4$	$V_6 \to C_7$, $V_6 \to C_5$, $V_5 \to C_7$, $V_5 \to C_6$	$V_6 \to C_7$, $V_5 \to C_7$, $V_6 \to C_6$, $V_3 \to C_6$, $V_3 \to C_5$, $V_1 \to C_6$,		
$E = 7.47$ eV	$V_6 \to C_7$, $V_6 \to C_6$, $V_5 \to C_6$, $V_4 \to C_7$, $V_3 \to C_7$		$V_6 \to C_7$, $V_4 \to C_7$, $V_3 \to C_7$	$V_3 \to C_6$, $V_4 \to C_6$, $V_2 \to C_7$	$V_2 \to C_7$, $V_5 \to C_6$
			Rb_2SnBr_6		
$E = 2.54$ eV	$V_1 \to C_1$, $V_2 \to C_1$, $V_3 \to C_1$	$V_5 \to C_1$, $V_6 \to C_1$ $V_3 \to C_1$		$V_1 \to C_1$, $V_2 \to C_1$	
$E = 5.13$ eV	$V_1 \to C_3$, $V_2 \to C_3$, $V_5 \to C_3$, $V_4 \to C_3$, $V_6 \to C_3$	$V_5 \to C_3$, $V_3 \to C_6$, $V_1 \to C_4$, $V_3 \to C_4$	$V_1 \to C_3$, $V_1 \to C_6$, $V_1 \to C_4$, $V_3 \to C_4$, $V_3 \to C_3$		
$E = 6.5$ eV	$V_1 \to C_7$, $V_2 \to C_7$, $V_3 \to C_7$, $V_4 \to C_4$ $V_5 \to C_4$	$V_6 \to C_7$, $V_6 \to C_5$, $V_5 \to C_7$, $V_6 \to C_4$	$V_1 \to C_6$, $V_4 \to C_5$, $V_3 \to C_6$, $V_6 \to C_7$, $V_5 \to C_7$	$V_6 \to C_4, V_2 \to C_5$	

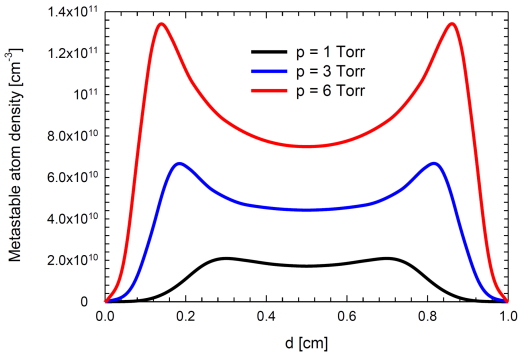

Fig. 11. Metastable atom density curves in the 2000th cycle CCRF argon dielectric barrier discharge as a function of d for different pressure values. These curves are cycle-averaged. (Fig. 3 from [16]).

TABLE VII

SEM EDS of oxidation elements [wt%] after 25 h furnace atmosphere–air (765°C) exposures. (Table V from [8])

Elements	Position of electron probe		
	1	2	3
oxygen	24.686	9.983	0
magnesium	0.015	0.056	0.141
silicon	4.149	3.626	2.925
chromium	0.161	0.236	0.264
manganese	5.722	6.536	9.473
nickel	7.074	6.745	5.617
iron	52.091	69.402	75.445

References

[1] V.P. Chornii, V.V. Boyko, S.G. Nedilko, O.V. Petrenko, V.M. Prokopets, K.V. Terebilenko, M.S. Slobodyanyk, *Acta Phys. Pol. A* **141**, 237 (2022).

[2] S. Basak, A. Ptok *Acta Phys. Pol. A* **143**, 195 (2023).

[3] S.I. Kuryshchuk, I.G. Orletskii, O.V. Shyrokov, D.V. Myroniuk, M.M. Solovan, *Acta Phys. Pol. A* **142**, 625 (2022).

[4] M. Ati, C. Enachescu, R. Bouamrane, *Acta Phys. Pol. A* **141**, 191 (2022).

[5] J. Merlin, A. Basherrudin Mahmud Ahmed, *Acta Phys. Pol. A* **141**, 516 (2022).

[6] A. Chatterjee, *Acta Phys. Pol. A* **141**, 183 (2022).

[7] P. Horodek, K. Siemek, M.N. Mirzayev, E.P. Popov, A.A. Donkov, M. Kulik, M. Turek, M. Bielewicz, *Acta Phys. Pol. A* **142**, 702 (2022).

[8] M.M. Rashidia, M.H. Idris, Z. Shayfull, A.H. Ahmad, M.M.A. Abdullah, P. Pietrusiewicz, M. Nabiałek, J. Garus *Acta Phys. Pol. A* **142**, 56 (2022).

[9] R.N. Vargas, A.C. Paschoarelli Veiga, R.R. Linhares, *Acta Phys. Pol. A* **143**, 47 (2023).

[10] B.A. Orlowski, K. Gwozdz, K. Goscinski, S. Chusnutdinow, M. Galicka, E. Guziewicz, B.J. Kowalski, *Acta Phys. Pol. A* **141**, 548 (2022).

[11] G.G. Konan, B. Karaçoban Usta, *Acta Phys. Pol. A* **142**, 539 (2022).

[12] Xinhua Zhang, Kok Jun Liew, Chun Shiong Chong, Xiaohong Cai, Zhidong Chang, Hao Jia, Peng Liu, Hua He, Wei Liu and Yuexian Li, *Acta Phys. Pol. A* **143**, 12 (2023).

[13] M. Skotniczny, D. Cekus, P. Kwiatoń, P. Kwiatoń, M. Šofer, *Acta Phys. Pol. A* **142**, 133 (2022).

[14] P. Horodek, K. Siemek, *Acta Phys. Pol. A* **142**, 697 (2022).

[15] L. Krache, M.A. Ghebouli, B. Ghebouli, M. Fatmi, T. Chihi, S.I. Ahmede, *Acta Phys. Pol. A* **143**, 3 (2023).

[16] A. Bouchikhi, *Acta Phys. Pol. A* **142**, 249 (2022).